Design of a Resonant Converter for Very Low-Frequency High-Voltage Test Systems

Zhiyu Cao, Norbert Fröhleke, Joachim Böcker
Institute of Power Electronics and Electrical Drives,
Paderborn University
33095 Paderborn, Germany

Abstract

With the rapid growth of decentralized energy generation from renewable resources, the connecting high-voltage cabling grid is also increasing. Therefore, a large demand on mobile high-voltage cable test systems results in the coming years. This paper deals with the development of a LCC resonant converter-based power supply scheme generating an 85 kV (RMS) sinusoidal test voltage at very low frequency of 0.1 Hz for testing of high voltage cables. The resonant converter is designed based on steady state AC analysis. The results are verified with experimental investigations conducted on a prototyping system.

1. Introduction

After introduction 20 years ago the very low-frequency (VLF) measuring technique for high-voltage test system (HVTS), has been accepted in standards HD 620-S1 in 1996 and IEC 60060-3-2006, recently [1]. In comparison with HVTS operating at 50 Hz the VLF-HVTS has considerable advantages in respect of volume, weight and energy consumption.

Regrettably, current VLF-based truesinus[1] generators use only the phase-shifted full-bridge inverter scheme [2] [3], which cannot make use of non-negligible winding capacitances of the high-voltage (HV) transformer windings and of the capacitors for static and dynamic control of the voltage stress on HV-rectifiers in the Cockcroft Walton voltage multiplier rectifier circuit (CW-multiplier). In order to overcome these drawbacks as well as to shrink volume, weight and cost with respect to magnetic components, a LCC resonant converter scheme operating at high switching frequency is a recommended topology for DC-DC applications [4] [5] [6]. Due to its buck and boost characteristics this topology is also very suitable for the complex load behaviour in this novel application.

As the LCC resonant converter is operated above the resonant frequency, ZVS is preserved for both legs. In order to generate a sinusoidal output voltage of 85 kV and 0.1 Hz, the electric energy stored in the HV-cable is controlled by LCC resonant converters and R-Controllers as shown in Fig.1.

[1] Truesinus is the Trademark of BAUR Prüf- und Messtechnik GmbH, Sulz / Austria.

This contribution is organized as follows: The system is briefly described in Chapter 2. For steady-state analysis of the converter, load characteristics are modelled using equivalent resistances given in Chapter 3. Based on the AC fundamental analysis technique, the steady state control characteristics of a LCC resonant converter are presented in Chapter 4. This design is verified through simulation and measurement on a prototype in Chapter 5.

2. System Description

As shown in Fig. 1 the VLF-HVTS comprises a positive subsystem, which generates the positive half-wave of a sinusoidal voltage of 85 kV / 0.1 Hz, and a negative one. Each subsystem consists of four functional modules: LCC resonant converter, HV-transformer, CW-multiplier, R-controller. Rectifier with a DC-link voltage U_{In} and HV-cable are the common parts of both subsystems. For converter development, only the electric characters of the HV-cable will be considered. Hence, it is simply modelled as a capacitive load, which has a maximum capacitance of 1.65 µF. As the positive and the negative subsystems have the same structures, only the positive one is outlined in the following description. The crucial functional modules of the system are presented below:

A. LCC resonant converter

A full-bridge topology is used for the resonant converter as shown in Fig. 1. Due to the operation above the resonant frequency, the turn-on action of transistors is guaranteed at zero volt-

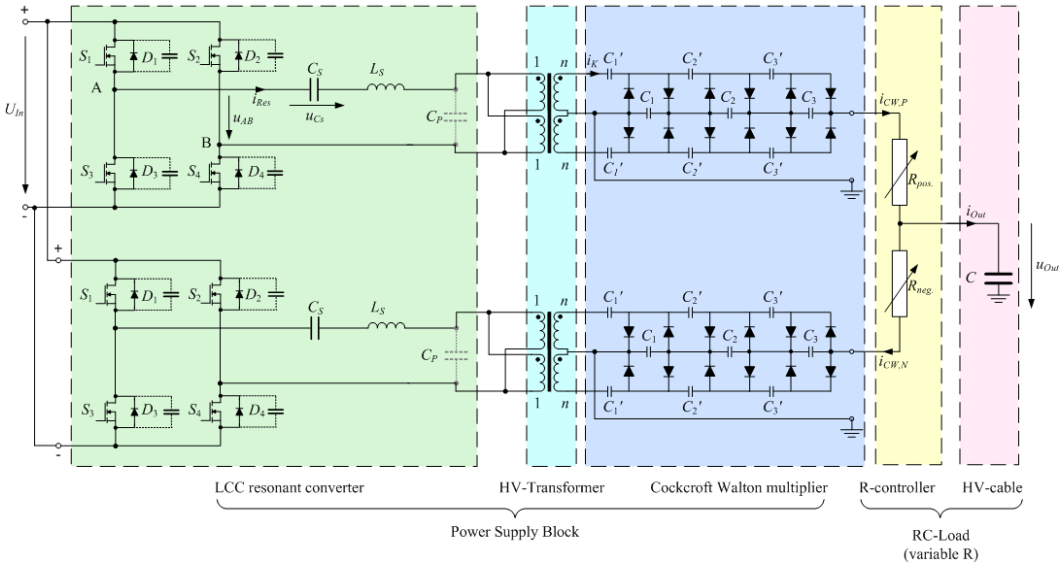

Fig. 1. Structure of the power circuit of a VLF-HVTS.

age and this applies also for the turn-off action, which is ensured by the parallel connected capacitors. The serial inductors L_S is formed by a physical inductor in combination with the transformer leakage inductance. The parallel capacitance C_P denotes the equivalent capacitance of the secondary winding capacitance of the HV-transformer added by capacitors of the HV-multiplier for voltage stress control of several connected diodes forming each shown rectifier.

The output power of the CW-multiplier, one part of which charges the HV-cable and the others is dissipated as losses by R-controller, is controlled through variation of set values: switching frequency and duty cycle of the LCC resonant converter.

B. HV-transformer and CW-multiplier

In high-voltage applications using resonant topologies, the size of a HV-transformer is essentially determined by the necessary isolation distances. In order to reduce the isolation voltage of the transformers, a combination of a transformer and a full-wave CW-multiplier is advantageous. However, as pointed out in [6], a three-stage CW-multiplier is recommended for the present case, so that losses and size of the cascade does not exceed the savings of the transformer.

As well known, all components of the CW-multiplier are stressed with the identical voltage $u_{stage} = u_{Out}/3$ except C_1', which has to withstand only half of it.

LCC resonant converter, HV-transformer and CW-multiplier constitute the power supply block, which injects electric energy into the HV-cable and R-Controller.

C. R-controller

As the power supply block is not bi-directional, the cable is discharged by the resistors R_{pos}.and R_{neg}, see Fig. 1. In order to guarantee a true sinusoidal voltage waveform, the resistors have to be carefully adapted. Such adjustable resistors, so-called R-controllers, are implemented as a chain of N HV-resistors. Each of them can be bypassed by an IGBT, see Fig. 2. Two of such R-controllers are required for the circuitry.

To ensure minimum loss in the R-controllers as long as the positive power supply block is charging the cable, R_{pos} should be set at zero and R_{neg} should be set at maximum value.

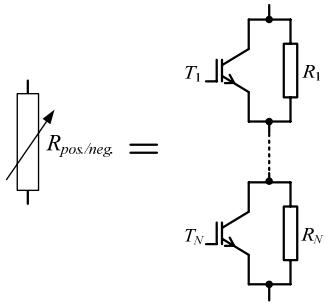

Fig. 2. Structure of R-controllers; $R_1 = R_2 = \cdots = R_N = R_0$, $R_{pos}/R_{neg} = k \cdot R_0$ ($k = 0, 1, \cdots, N$).

3. Description of the Load Characteristic

With a required sinusoidal test voltage

$$u_{Out}(t) = \hat{U} \cdot \sin(\omega t) = \hat{U} \cdot \sin(2\pi f t) \quad (1)$$

the electric energy

$$e_C(t) = \frac{1}{2} C \cdot u_{Out}{}^2(t) \quad (2)$$

has to be stored in the HV-cable assuming a lumped equivalent capacitance for the distributed cable capacitance. The charging or discharging power of the HV-cable is:

$$p_C(t) = \frac{de_C(t)}{dt}. \quad (3)$$

As the output voltage of the VLF-HVTS has a very low frequency of 0.1 Hz and the resonant converter is operated in the range of tens of kilohertz, the quasi steady-state load behaviour at a certain instant t can be described using an varying equivalent resistance

$$R_{equ}(t) = \frac{u_{Out}(t)}{i(t)} = \frac{u_{Out}{}^2(t)}{p_C(t)}. \quad (4)$$

As mentioned in Chapter 2, as long as the positive resonant converter is operated ($i_{CW,P} > 0$) the resistance of the positive R-controller is always zero ($R_{pos} = 0$) and the negative R-controller is at its maximum ($R_{neg} = R_{max}$). Thus, a total effective load resistance R_L results from the parallel connection of the equivalent resistance from (4) and R_{max}:

$$R_L(t) = R_{equ}(t) \,||\, R_{\max} \quad (5)$$

Ignoring all further losses, the resonant converter has to supply the output power:

$$p_{conv,out}(t) = p_C(t) + p_{R-ctrl}(t) \quad (6)$$

where

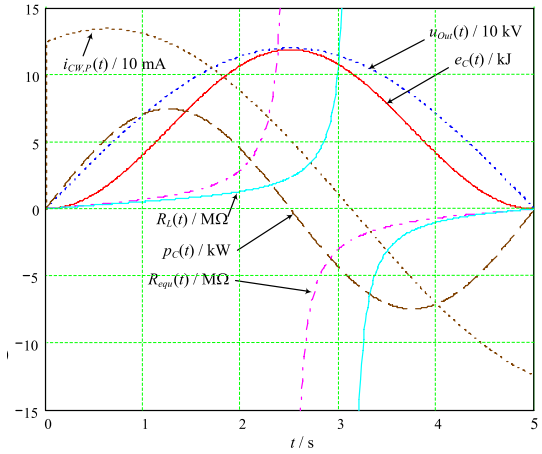

Fig. 3. Characteristics during the positive half period of the test voltage

$$p_{R-ctrl}(t) = \frac{u_{out}{}^2(t)}{R_{\max}} \quad (7)$$

Parameters of equations (1) to (7), switching frequency f_S and duty cycle d are defined according to the following technical specifications:

$\hat{U} = 120$ kV	$f = 0.1$ Hz
$R_0 = 11.2$ kΩ	$N = 210$
$R_{\max} = N \cdot R_0 = 2.35$ MΩ	$C = 0 \cdots 1.65$ µF
$f_S = 27 \cdots 40$ kHz	$d = 0 \cdots 100\%$

Four typical operation points at maximal rated load capacitance are defined as shown in Table 1 as representatives for further analysis in Chapter 4:

Tab. 1. Typical operation points (OP) of VHTS

OP	u_{Out} / kV	$i_{CW,P}$ / mA	R_L / kΩ	Comments
1	11.7	128	91.3	Small u_{out}
2	46	135	341.5	Max. $i_{CW,P}$
3	100	112	894.3	Max. $p_{converter,out}$
4	120	51	2350	Max. u_{out}

4. Converter Design Based on AC Analysis Using Fundamental Components

Ignoring all losses and simplification of each subsystem yields the equivalent circuit illustrated in Fig. 4.a, with all components being transformed to the primary side of the HV-transformer. As mentioned in [5], [7] and [8], the behaviour of LCC resonant converters with capacitive output filter can be furthermore simplified through an equivalent AC circuit as shown in Fig. 4.b.

Using these findings and considering the voltage transfer ratio of the HV-transformer ($1{:}n$) as well as the k-stage CW-multiplier ($k = 3$), the conduction angle θ can be calculated through (see Fig. 4.c):

$$\theta = 2 \cdot \tan^{-1} \sqrt{\frac{\pi}{2 \cdot f_{S,N} \cdot \alpha \cdot Q}}, \quad (8)$$

where $f_{S,N}$ is the normalized switching frequency, α is the ratio of C_P to C_S, and Q is the normalized load resistance as follows:

$$f_{S.N} = f_S / f_0 \quad (9)$$

$$f_0 = 1/2\pi\sqrt{L_S \cdot C_S} \quad (10)$$

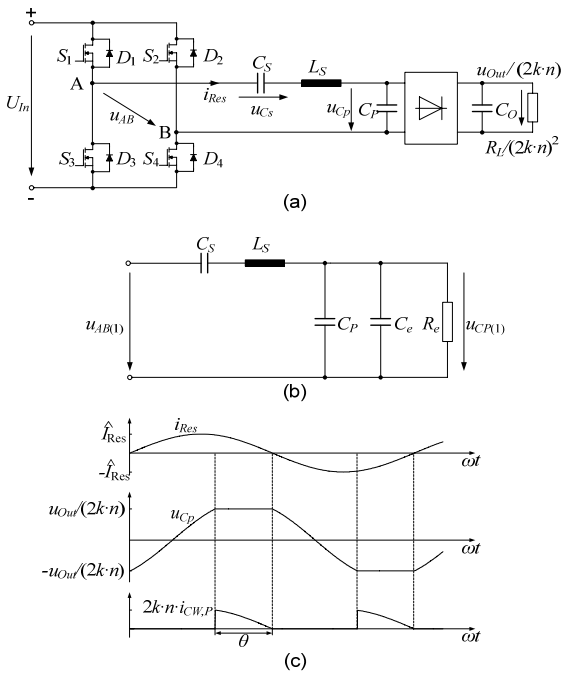

Fig. 4. Simplified circuit of a subsystem through transforming all components to primary side of HV-transformer, C_O denotes the equivalent capacitance of the CW-multiplier (a), AC equivalent circuit (b) and its current as well as voltage waveforms (c).

$$\alpha = C_P / C_S \tag{11}$$

$$Q = \frac{R_L}{n^2 \cdot (2k)^2 \cdot \sqrt{L_S / C_S}} \tag{12}$$

The voltage waveform coefficient k_V and the phase angle β between the first harmonic of the parallel capacitor voltage $u_{Cp(1)}$ and its current $i_{Cp(1)}$ can be approximated according to [8] by:

$$k_V = \frac{\hat{u}_{Cp(1)}}{U_O/(n \cdot 2k)} \approx 1 + 0.27 \cdot \sin(\frac{\theta}{2}) \tag{13}$$

$$\beta \approx -0.439 \cdot \sin(\theta) \tag{14}$$

Using these parameters, the equivalent resistor R_e and the equivalent capacitance C_e of equivalent circuit according to Fig. 4b can be obtained as

$$R_e = \frac{{k_V}^2}{2 \cdot (n \cdot 2k)^2} \cdot R_L \tag{15}$$

$$C_e = \frac{2 \cdot (n \cdot 2k)^2}{\omega \cdot R_L \cdot {k_V}^2} \cdot \tan|\beta| \tag{16}$$

So we obtain the AC voltage ratio of $u_{Cp(1)}$ to $u_{AB(1)}$:

$$k_{21} = \frac{1}{\sqrt{[1-\alpha \cdot (f_{SN}^2 - 1) \cdot (1 + \frac{\tan|\beta|}{\omega \cdot C_P \cdot R_e})]^2 + [\alpha \cdot (f_{SN}^2 - 1) \cdot \frac{1}{\omega \cdot C_P \cdot R_e}]^2}} \tag{17}$$

Since the amplitude of the first harmonic of the voltage $u_{AB(1)}$ can be deduced from:

$$\hat{u}_{AB(1)} = \frac{4}{\pi} \cdot \sin(\frac{\pi}{2} \cdot d) \cdot U_{In}\,, \tag{18}$$

the output voltage results to

$$u_{Out} = \hat{u}_{AB(1)} \cdot k_{21} \cdot \frac{n \cdot 2k}{k_V} = \frac{4}{\pi} \cdot \sin(\frac{\pi}{2} \cdot d) \cdot k_{21} \cdot \frac{n \cdot 2k}{k_V} \cdot U_{In}\,. \tag{19}$$

According to (19), the control characteristics for the four typical operation points can be computed as shown in Fig. 5. After a number of iterative investigations, a combination of n = 15, C_L = 270 nF and L_S = 270 µH proved as optimal parameters to fulfill the technical specification and

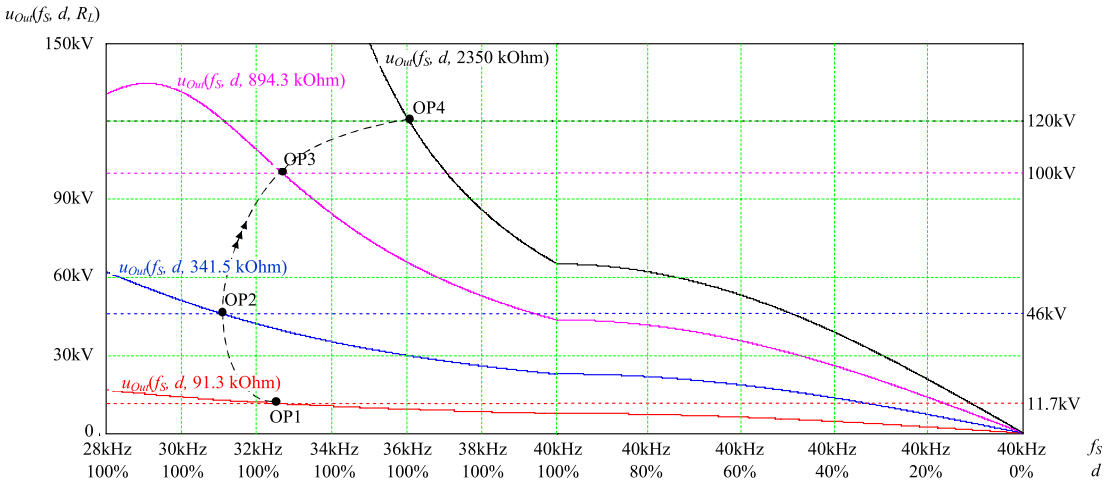

Fig. 5. Control characteristics for four typical operation points according to the equivalent load resistances as defined in Table 1.

constraints:

- Minimize RMS-value and amplitude of i_{Ls} in order to reduce volume, weight and cost of series inductor and the HV-transformer;
- Minimize the amplitude of u_{Cs} in order to realize C_S conveniently using available components.

For shorter HV-cables with lower capacitance values, similar control characteristics can also be derived using this analysis. However, due to the time varying load characteristics and the large range of output voltage, it is more confusing to illustrate all graphs of various cable capacitances within one figure (see Fig. 5).

In order to overcome this difficulty, the output voltage u_{Out} and the output current of the positive CW-multiplier $i_{CW,P}$ at a constant switching frequency $f_{S,i}$ and duty cycle d_i can be rewritten with functions to R_L by:

$$u_{Out} = f(R_L) \tag{20}$$

$$i_{CW,P} = g(R_L) \tag{21}$$

If R_L varies between 0 and 2.35 MΩ, a set of control characteristics at respective switching frequencies f_S and duty cycles d results as illustrated in Fig. 6.

According to the load analysis in Chapter 3 the current $i_{CW,P}$ can also be related as a function of u_{Out}, which is illustrated in Fig. 6 for various ratting of C_L and set values of f_S and d:

$$i_{CW,P} = h(u_{Out}) \tag{22}$$

Two situations are critical: maximum capacitance (1.65 µF) and the no load condition (HV-cable is not connected). At maximum load capacitance shown in Fig. 5, the resonant converter is operated in frequency modulation mode with a constant duty cycle of 1. At no load operation, however, it begins with a minimum duty cycle at 40 kHz. At around 65 kV output voltage the duty cycle reaches the maximum value of 1 and the frequency modulation begins. The area between these two critical modes builds the operation area of the VLF-HVTS.

5. Simulative and Experimental Results

For validation of derived analytic results gained by AC analysis using fundamental components, the positive part of this system shown in Fig.1 was simulated in Matlab/Simulink. It was supplemented by an additional Plecs toolbox, which provides a graphical user interface to build simulation models of power electronic circuits, efficiently. Because of the high cost in manufacturing HV-resistors, only one load resistor was manufactured for testing. The test resistor has a value of $R_L = 977.6$ kΩ, rated between equivalent resistances of OP3 and OP4 according to Tab. 1.

Measured and simulated results are shown in Fig. 7. Ignoring all kinds of losses conformable results are obtained between theoretic analysis (u_out_Theo) and simulation (u_out_Sim1). Taking the known part of semiconductor conduction and ohmic losses into account in the simulation model, the simulated output voltage (u_out_Sim2) is lower as with the theoretic analysis. As the losses due to skin effect, stray capacitances in the high voltage side and switching actions of HV-diodes are difficult to consider in the simulation module, the output voltage from experiment (u_out_exp) is of course lower than

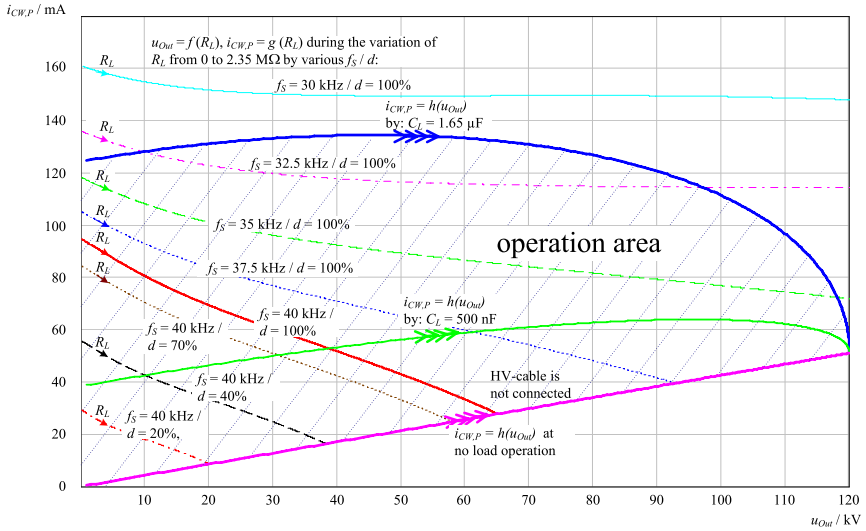

Fig. 6. Working tracks of the HVTS by various capacitance values of the HV-cable.

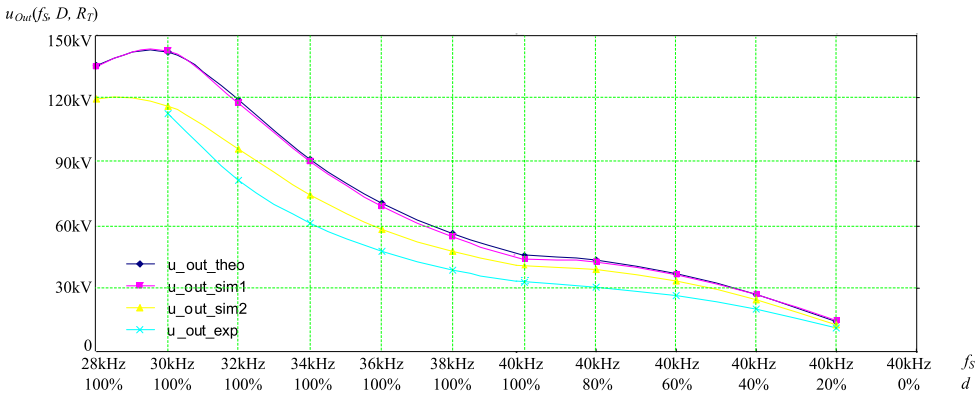

Fig. 7. Control characteristic lines of the in table I defined four equivalent load resistances as well as the four typical working points.

the second simulation result.

According to Chapter3, this test resistor represents the load character of a 1.65 µF cable capacitance at the time instance of $t = 1.668$ s. At this instant the desired output voltage and the output current of CW-multiplier should be: $u_{Out} = 104$ kV and $i_{CW,P} = 106$ mA. As shown in Fig.7 this point of operation is set by adjusting the switching frequency of f_S to 31 kHz and duty cycle d to 100%. This fulfils the design specifications.

6. Conclusion

In this contribution the LCC resonant topology is successfully used as a novel power supply solution for a VLF-HVTS. For converter design the following simplifications of the VLF-HVTS are proved to be efficient:

- Simplification of the load behaviours by using equivalent resistances;
- Simplification the CW-multiplier by using a rectifier with an equivalent capacitive output filter;

Based on the both simplifications the major operation characteristics of the VLF-HVTS are efficiently derived through conventional AC analysis technique using fundamental components. Using an iterative design procedure based on this analysis in conjunction with the constraint to minimize stress quantities of resonant tank components leads to a good parameter combination out of technical and economical view. Results of the theoretical analysis are verified by simulation and experiment.

Acknowledgement

Thanks belong to BAUR Prüf- und Messtechnik GmbH, Sulz / Austria for funding this project as well as our project partners.

References

[1] VLF related Standards: VDE DIN 0276-620, IEEE P400.2, VDE DIN 0276-621, CENELEC HD 620 and CENELEC HD 621.

[2] T. F. Wu, H. P. Yang and C. M. Pan: “Analysis and design of variable frequency and phase-shift controlled series resonant converter applied for electric arc welding,” in Proc. 21st IEEE IECON, vol. 1, 1995, pp. 656-661.

[3] R. L. Steigerwald, R. W. De Doncker and H. Kheraluwala: “A comparison of high-power dc-to-dc soft-switched converter topologies,” IEEE Trans. on Industry Applications, vol. 32, pp.1139-1145, 1996.

[4] S. D. Johnson, A.F. Witulski and R.W. Erickson: “Comparison of Resonant Topologies in High-Voltage DC Applications,” in Proc. IEEE Applied Power Electronics Conference, 1987, pp. 263-274.

[5] F. S. Cavalcante and J.W. Kolar: “Design of a 5kW High Output Voltage Series-Parallel Resonant DC-DC Converter,” in Proc. 34th IEEE Power Electronics Specialists Conf., 2003, vol. 4, pp. 1807-1814.

[6] H. Osterholz and C. Paul: “Untersuchung resonanter Hochspannungs-kaskaden unterschiedlicher Stufenzahl,” in SIMPLORER Workshop 2001.

[7] R. L. Steigerwald: “Analysis of a Resonant transistor DC-DC converter with capacitive output filter,” IEEE Trans. on Industrial Electronics, Vol. IE-32, no. 4, November 1985, pp. 439-444.

[8] G. Ivensky, A. Kats and S. Ben-Yaakov: “A Novel RC Model of Copacitive-loaded Parallel and Series-Parallel Resonant DC-DC Converters,” in Proc. of the 28th IEEE Power Electronics Specialists Conference, St. Louis, Missouri, USA, vol. 2, 1997, pp. 958-964.